Journal of Renewable Materials

Tech Science Press

DOI: 10.32604/jrm.2023.030599

ARTICLE

CoS Nanosheets Coated with Dopamine-Derived Carbon Standing on Carbon Fiber Cloth as Binder-Free Anode for Li-ion Batteries

Lianyuan Ji[1], Mingchen Shi[1], Zengkai Feng[2] and Hui Yang[1,*]

[1]College of Materials Science and Engineering, Nanjing Tech University, Nanjing, 211816, China

[2]Department of Design, Huadingju Engineering Co., Ltd., Tianjin, 300041, China

[*]Corresponding Author: Hui Yang. Email: yanghui@njtech.edu.cn

Received: 14 April 2023 Accepted: 02 June 2023 Published: 11 March 2024

ABSTRACT

Cobalt sulphides attract much attention as anode materials for Li-ion batteries (LIBs). However, its poor conductivity, low initial column efficiency and large volume changes during cycling have hindered its further development. Herein, novel interlaced CoS nanosheets were firstly prepared on Carbon Fiber Cloth (CFC) by two hydrothermal reactions followed with carbon coating via carbonizing dopamine (CoS NS@C/CFC). As a freestanding anode, the nanosheet structure of CoS not only accommodates the volume variation, but also provides a large interface area to proceed the charge transfer reaction. In addition, CFC works as both a three-dimensional skeleton and an active substance which can further improve the areal capacity of the resulting electrode. Furthermore, the coated carbon combined with the CFC work as a 3D conductive network to facilitate the electron conduction. The obtained CoS NS@C/CFC, and the contrast sample prepared with the same procedure but without carbon coating (CoS NS/CFC), are characterized with XRD, SEM, TEM, XPS and electrochemical measurements. The results show that the CoS NS@C/CFC possesses much improved electrochemical performance due to the synergistic effect of nanosheet CoS, the coated carbon and the CFC substrate, exhibiting high initial columbic efficiency (~87%), high areal capacity (2.5 at 0.15 mA cm^{-2}), excellent rate performance (1.6 at 2.73 mA cm^{-2}) and improved cycle stability (87.5% capacity retention after 300 cycles). This work may provide a new route to explore freestanding anodes with high areal specific capacity for LIBs.

KEYWORDS

Lithium-ion battery; cobalt sulfide; carbon coating; carbon fiber cloth; freestanding anode

1 Introduction

Lithium-ion batteries (LIBs) have been dominating the power supply markets for electronic devices, electric/hybrid vehicles and energy storage systems for the past several decades [1–4]. With the increasing demands of various applications, current LIBs no longer meet the requirements since the energy densities are partially restricted by the low capacity of Graphites (372 Ah kg^{-1} and ~837 Ah L^{-1}) [5]. In the meantime, the popularity of wearable devices requires flexible LIBs based on flexible self-supporting electrodes [6,7]. Huge efforts have been applied to explore novel electrode materials with high specific capacity and excellent electrochemical performance [8–10], in which transition metal sulfides with high available capacity, such as MoS_2 [11], MnS [12], NiS [13], FeS_2 [14] and CoS_2 [15] have

attracted much attention, since they could be fabricated with various facile methods and easily deposited on flexible supports such as carbon paper/cloth to make flexible self-standing electrodes. Among those sulfides, cobalt sulfides, possessing a specific capacity as high as 500–800 mAh g^{-1}, have attracted much attention in recent years [16–18].

Currently cobalt sulfides face several challenges, including poor rate performance caused by their inferior electric/ionic conductivity, inadequate cycling life originating from the large volume expansion that occurred during lithiation [19], and low initial columbic efficiency, which is the common issue of transition reaction based electrode materials. Elaborate nano-structures, including hierarchitectures [20], hollow nanoparticles [21], nanosheets [22], nanotubes [23], etc., have been introduced to shorten the electron/ion transport path and house the volume expansion, whereas the inherent poor conductivity of cobalt sulfides still limits the rate of electron transfer [21,24]. Therefore, conductive carbon coating has been applied to improve the conductivity, meanwhile, to host some volume variation during cycling, resulting in much improved electrochemical performance and cyclic stability [10,25–27].

In this paper, a self-supporting electrode consisting of carbon-coated cobalt sulphide nanosheets (denoted as CoS NS@C/CFC) was synthesized on Carbon Fibre Cloth, in which the coated carbon was derived from dopamine. It has to be addressed that CFC works as both active and support material in this context. Benefit from the synergistic effects of cobalt sulfide nanosheets, coated carbon film and CFC, the anode exhibits high areal capacity (2.5 at 0.15 mA cm^{-2}), excellent rate performance (1.6 at 2.73 mA cm^{-2}) and improved cyclic stability (87.5% capacity retention after 300 cycles). And moreover, the CoS-based self-standing electrode presents a relatively high initial columbic efficiency, up to 87%, which is comparable to many graphite-based anodes.

2 Experimental

2.1 Synthesis of Co-Precursor NS/CFC

In a Teflon autoclave, 0.5821 g $Co(NO_3)_2{\cdot}6H_2O$ (2 mmol) and 0.5607g methenamine (4 mmol) were dissolved into 40 mL methanol, then a piece of Carbon Fiber Cloth (CFC, 25 mm * 50 mm) was introduced. The autoclave was maintained at 180˚C for 12 h. The co-precursor NS grown on CFC was obtained, washed several times with DI water and then vacuum-dried overnight. The carbon fiber cloth, with the areal density of 15.5 mg cm^{-2}, was purchased from Senyou Charcoal Fiber Co., Nantong, China (Battery-grade).

2.2 Synthesis of CoS NS/CFC

The CoS NS/CFC was obtained by placing the obtained Co-precursor NS/CFC into an ethanol solution containing 0.20 g thioacetamide. The above mixture was placed into an autoclave and maintained at 160˚C for 3 h. The resulting product was collected, washed several times with distilled water/ethanol and then dried overnight at 60°C under vacuum. The average loading of CoS NS was measured as 1.3 ± 0.2 mg cm^{-2}.

2.3 Synthesis of CoS NS@C/CFC

The aforementioned CoS NS/CFC was immersed into the solution prepared by dissolving 0.06 g dopamine hydrochloride into 50 mL Tris buffer (pH 8.5), followed by magnetically stirring for 4 h. The obtained CoS NS@Polydopamine (PDA)/CFC sample was then washed with ethanol/distilled water several times, and dried at 60°C in a vacuum oven. Finally, the CoS NS@PDA/CFC was treated at 550˚C under Nitrogen atmosphere for 2 h to carbonize the coated PDA, leading to the formation of the CoS NS@C/CFC composite. The average loading of CoS NS was measured as 1.3 ± 0.2 mg cm^{-2}.

2.4 Characterization

Regarding the homemade samples, their crystal structure information was examined by X-ray diffraction (XRD, Rigaku with Cu Kα radiation). The microscopic morphology and structure of the material were obtained by field emission scanning electron microscopy (FE-SEM, Hitachi S-4800) and transmission electron microscopy (TEM, FEI Talos F200). X-ray photoelectron spectra (XPS) were measured using an X-ray photoelectron spectrometer (Kratos Axis Ultra DLD).

2.5 Electrochemical Measurements

The electrochemical performance of CoS NS/CFC and CoS NS@C/CFC (1 cm^{-2}) as binder-free anodes for LIBs was examined using CR2032 coin-type cells, which were assembled in a dry box with metallic Lithium foil as a reference/counter electrode. The electrolyte ration is 1 M $LiPF_6$ dissolved in ethylene carbonate-dimethyl carbonate (1:1 vol%). Using a CHI660E electrochemical workstation, cyclic voltammetry was scanned at 0.1 mV s^{-1} and electrochemical impedance spectroscopic (EIS) analysis was carried out at the open circuit potential with an amplitude of 10 mV over the frequency range from 10 to 100 KHz. Galvanostatic charge-discharge tests were run at different current densities in the range of 0.18–2.73 mA cm^{-2} over the potential range of 0.01–3.00 V *vs*. Li^+/Li using a Neware battery tester.

3 Results and Discussion

3.1 Synthesis and Surface Morphology of CoS NS@C/CFC

The preparation of CoS NS@C/CFC is illustrated in Fig. 1a. Firstly, the interlaced Co-precursor nanosheets were grown on the Carbon Fiber Cloth (denoted as Co-precursor NS/CFC) by the hydrothermal treatment in hexamethylenetetramine dissolved with methanol. The Co-precursor nanosheets were grown randomly and densely on the CFC in the appearance of black fungi (Fig. 1b). Secondly, the CoS nanosheets/CFC (marked as CoS NS@CFC) was fabricated by the sulfuration of Co-precursor NS@CFC using thioacetamide, which are converted to CoS NS standing on CFC without changing the morphology as depicted in Fig. 1c. Thirdly, the CoS NS@CFC was immersed into dopamine solution to coat polydopamine (PDA) onto CoS nanosheets. Lastly, PDA was transformed into thin carbon films by an annealing treatment under Nitrogen atmosphere to obtain the target sample CoS NS@C/CFC. The PDA coating and consequent annealing treatment generate thin N-doped carbon films on the surface of CoS NS which consists of multiple self-aggregated nanoparticles (Figs. 1d–1e).

The corresponding EDS mapping images from Figs. 1f–1j show the homogeneous dispensation of C, N, Co and S within the obtained target particles. Some CoS NS/CFC and CoS NS particles were scratched from the CFC support to further explore their microstructure via TEM (Figs. 2a–2b). The carbon films converted from PDA (denoted as C-PDA) are evenly coated on the CoS particles (Fig. 2a), which are well consistent with the SEM observation. Both values of the lattice spacing marked in the HRTEM images (Figs. 2c–2d) are calculated as 0.25 nm, belonging to the (101) lattice plane of hexagonal CoS [28].

3.2 Structural Characterization

XRD patterns of CFC, CoS NS/CFC and CoS NS@C/CFC are presented in Fig. 3. The two major diffraction peaks at about 25° and 44° (marked by heart) correspond to the Carbon Fiber Cloth. For the CoS NS/CFC sample, diffraction peaks detected at 30.2°, 35.2°, 47° and 54.3° (square) could be indexed into the hexagonal CoS (JCPDS:75-605) [29]. No other typical diffraction peak is detected, demonstrating that the synthesized CoS NS/CFC composites are of high purity. The XRD pattern of CoS NS@C/CFC shows no difference with that of CoS NS/CFC samples, which could be explained by the characteristics of amorphous carbon [30] as well as its small amount.

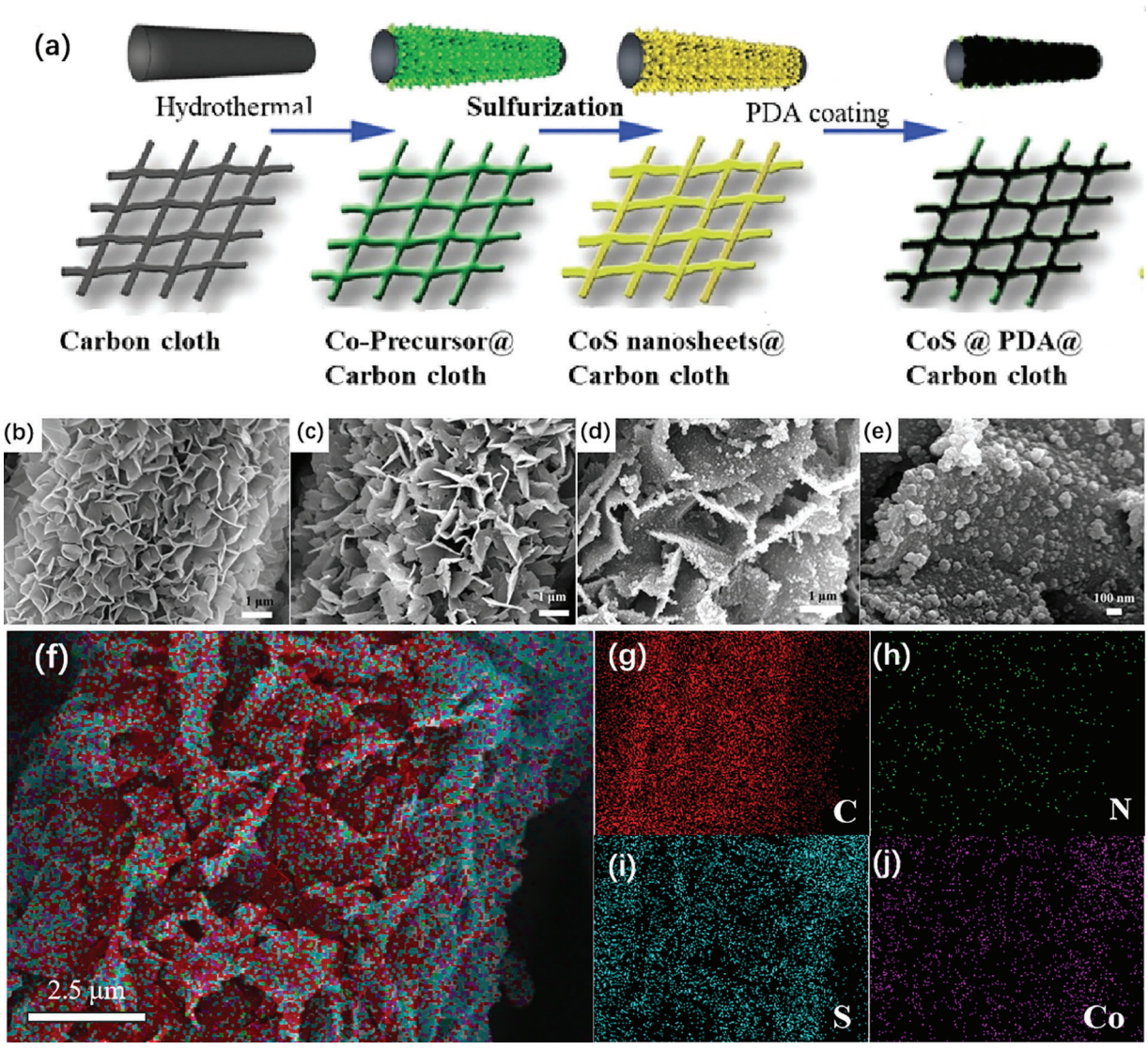

Figure 1: (a) Diagram of the synthesis of CoS NS@C/CFC and SEM inspections of (b) Co-precursor NS/CFC (c) CoS NS/CFC and (d) CoS NS@C/CFC (e) CoS NS@C/CFC at 60000× magnification and (f, g, h, i, j) the corresponding EDS maps showing the uniform distribution of C, N, S and Co in CoS NS@C/CFC

3.3 X-Ray Photoelectron Spectroscopy Analysis

In order to learn more about the elemental composition as well as their chemical states of the superficial layer of CoS NS@C/CFC, XPS analysis was employed and the obtained wide-scan spectrum (Fig. 4a) indicates the existence of four elements, i.e., C, N, Co and S [31,32]. The XPS spectrum of high-resolution C 1s is shown in Fig. 4b, where the three anti-convolution peaks at 289.1, 285.7 and 284.7 eV can be claimed to C-N, C-S and C=C/C-C bonds. This implies the presence of an N-containing group on the carbon atom [33,34]. The N 1s spectrum (Fig. 4c) shows three distinct peaks at 401.4, 400.2 and 399.0 eV associated with graphitic-N, pyrrolic-N and pyridinic-N, respectively. That means the PDA-precursor derived nitrogen has been integrated into the carbon films successfully, which has been proved

to improve the electrochemical performance via enhancing the conductivity of the resulting active materials [26]. In the Co 2p XPS spectrum (Fig. 4d), two fitted peaks at 798.3 and 782.3 eV, are indexed to Co $2p_{1/2}$ and $2p_{3/2}$, respectively. The other two peaks can be indexed to their satellite peaks [23,35]. The S 2p spectrum (Fig. 4e) presents two fit peaks at 164.9 and 163.8 eV, which are assigned to S $2p_{1/2}$ and $2p_{3/2}$, respectively. In addition, two fit peaks at 169.9 and 168.8 eV are corresponded to the S-N/S-O bonds coming from the incomplete sulfurization of the Co-precursor and the short exposure of the sample in air [36].

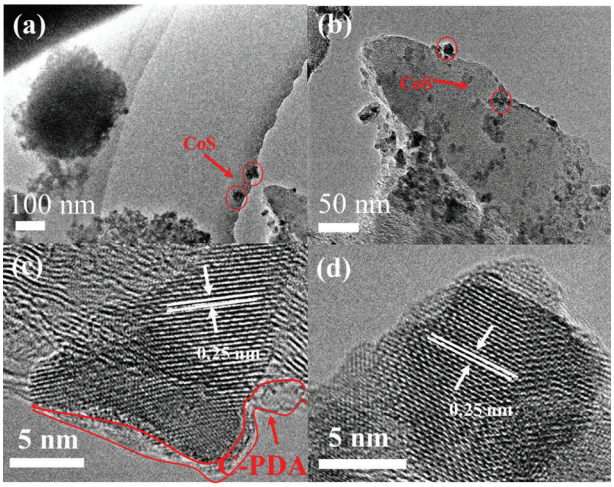

Figure 2: TEM and HRTEM images of (a, c) CoS NS@C/CFC and (b, d) CoS NS/CFC

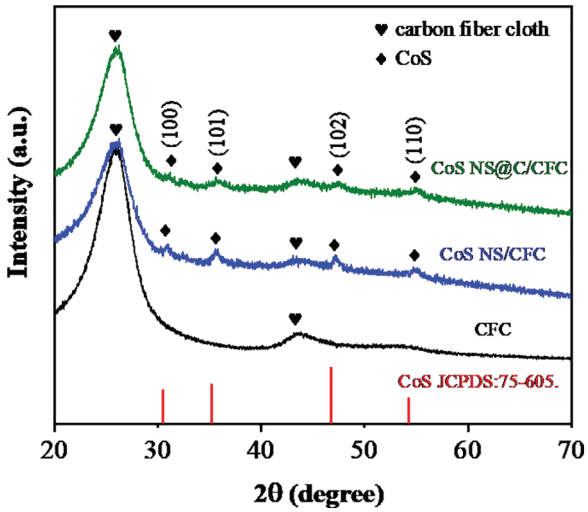

Figure 3: XRD patterns of CFC, CoS/CFC and CoS NS@C/CFC

3.4 Electrochemical Performance

Figs. 5a–5b illustrate the first three cycles of CV curves swept at 0.1 mV s^{-1} within 0.01 to 3.0 V *vs*. Li^+/Li for CoS NS@C/CFC and CoS NS/CFC electrodes. The CV curves of CoS NS@C/CFC exhibit the characteristic peaks of both CC and CoS components (Fig. 5a). The 1st cathodic scan starts from 1.7 V,

and shows a peak at 1.3 V which can be attributed to the initial insertion of lithium, together with the subsequent Co displacement to form Li_2S. While another small peak at around 1.0 V, followed with gradually increasing cathodic currents till 0 V, can be claimed as the characteristic peaks of CC support (Fig. S1a), which turns to anodic currents in the reverse scan. The role of the CFC and its lithium storage mechanism are discussed in the Supplementary Materials. The peak detected at 2.0 V corresponds to the oxidation of metallic Co to Cobalt sulfides. While the peak detected at 2.4 V can be claimed to the fully de-lithiation of Li_2S [35]. The peak at 1.8 V may be attributed to the reduction of newly formed sulfur in the subsequent cathodic scan ($S + 2e^- \rightarrow S^{2-}$) [37]. In the subsequent scans, the reduction peak at 1.3 V shifts to a higher potential, indicating some uncertain irreversible reactions occurred in the 1st cycle which can be claimed to form the solid electrolyte interphase film [38]. The CV curves of the 2nd and 3rd cycles are almost overlapped, demonstrating good redox reversibility and high stability for the CoS NS@C/CFC electrode. The CV curve of CoS NS/CFC electrode illustrates the similar characteristic peaks with that of CoS NS@C/CFC but with less reversibility, suggesting both electrodes share the same lithiation/delithiation processes. Figs. 5c–5d show the charge/discharge behaviors of CoS NS@C/CFC and CoS NS/CFC electrodes at 0.92 mA cm^{-2} within 0.01 to 3.0 V, exhibiting the 1st reversible capacity of 2.25 and 2.0 mAh cm^{-2}, respectively. Meanwhile, the charge-discharge curves of both electrodes are consistent with their CV curves. The CoS NS@C@CFC shows higher initial coulombic efficiency (CE) than CoS NS@CFC, 87% *vs*. 81%, agreeing well with what we concluded previously that the former sample exhibits better reversibility in CV scan than the later one. Since the low initial columbic efficiency is the common issue of transition reaction based electrode materials, it has to be addressed that the columbic efficiency of 87% obtained here is comparable to that of many commercialized graphite anodes, and is much higher than that of many reported CoS-based anodes in the literatures [15,39,40]. The cycling stability and coulombic efficiency of CoS NS@C/CFC and CoS NS/CFC cells tested at 0.91 mA cm^{-2} are illustrated in Fig. 6a. Obviously the CoS NS@C/CFC anode presents better capacity retention than the CoS NS/CFC anode. The initial areal capacity of the CoS NS@C/CFC anode decreases slightly after the first cycle and then maintains at around 2.25 mAh cm^{-2} till 100 cycles, exhibiting the capacity retention of nearly 98% compared to the first cycle. However, the initial areal capacity of the CoS NS/CC anode only reaches 1.98 mAh cm^{-2}, and remains 1.58 mAh cm^{-2} after 100 cycles, which has only 80% capacity retention. It can be seen that the CoS NS@C/CFC anode shows much better cycle stability than the CoS NS/CC anode. To further explore the reason for the superior cycle stability of CoS NS@C/CFC anode, the morphology of the CoS NS@C/CFC and CoS NS/CFC anode after 100 cycles was investigated by SEM (Figs. S2a–S2d). Despite the expected change of morphology due to the reduction of CoS NS and the formation of SEI, the carbon fiber is still covered by the nanosheets (Figs. S2a and S2b) [41,42]. However, Figs. S2a–S2d show that the nanosheets are significantly reduced. This indicates the strong protective effect of carbon film in CoS NS@C/CFC anode during cycling. The rate performance of the CoS NS@C/CFC electrode is evaluated under the current density of 0.18, 0.46, 0.91, 1.82, and 2.73 mA cm^{-2} (Fig. 6b), the obtained areal specific capacities are 2.0, 1.8, 1.6, 1.4, and 1.3 mAh cm^{-2}, respectively, which are better than those of CoS NS/CFC electrode. In addition, when the current density backs to 0.18 mA cm^{-2}, the specific capacity can be recovered to 2.0 mAh cm^{-2}, proving the excellent structure stability of CoS NS@C/CFC. It is worth noting that even at 1.82 mA cm^{-2}, the CoS NS@C/CFC anode still shows a high capacity retention of ~87.5% after 300 cycles. The CFC contribution is removed from the Figs. 6a and 6c, and the corresponding figures are presented in Figs. S4a and S4b to clarify the available capacity provided by CoS NS@C during the cycle life test.

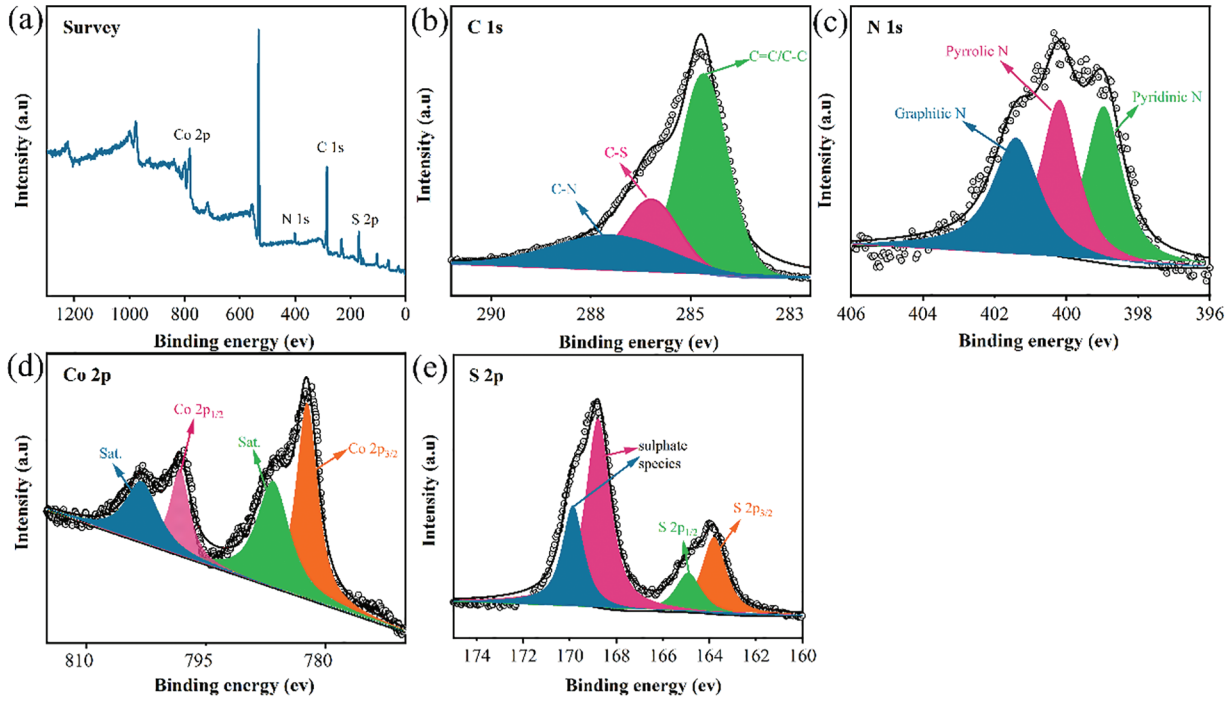

Figure 4: (a) The wide-scan spectrum (b) C 1s (c) N 1s (d) Co 2p and (e) S 2p X-ray photoelectron spectra of CoS NS@C/CFC composites

In order to further explore the Li^+ storage mechanism for CoS NS@C/CFC, the CV curves at different scan rates ranging from 0.2 to 1 mV s^{-1} are obtained and presented in Fig. 7a. It is well known that the Li^+ storage of the anode materials originates from two modes, diffusion-controlled process and pseudo-capacitance behavior, which can be estimated by the following equation:

$$i = av^b \tag{1}$$

The b value of 0.5 implies the diffusion-controlled process, while of 1 means pseudocapacitance behavior. In Fig. 7b, the b values are 0.69 (peak 1) and 0.64 (peak 2), indicating that both contribute the overall capacity, which can be further determined by the following equation [43,44]:

$$i(V) = k_1 v + k_2 v^{1/2} \tag{2}$$

Solving for the values of k_1 and k_2 at each potential obtains the contribution of the capacitive and diffusion currents. Figs S3a–S3e compare the fitted CV curves based on the capacitive current with the original CV curves at all scan rates. The contribution from the capacitive were calculated as 55.93%, 65.74%, 71.54%,79.30% and 86.40% at scan rates of 0.2 to 1.0 mV s^{-1}, respectively (Fig. S3f). Obviously as the scan rate increases, the capacitive behavior contributes more to the capacity. On the one hand, the CoS NS *in-situ* growth on the surface of CFC reduces their agglomeration, which increases the active sites for lithium storage and provides more interface area for the charge-transfer reactions. On the other hand, the abundant surface groups derived from carbonization also provide adsorption sites for lithium ions and increase the capacitive behavior, leading the extremely excellent rate performance of CoS NS@C/CFC electrode.

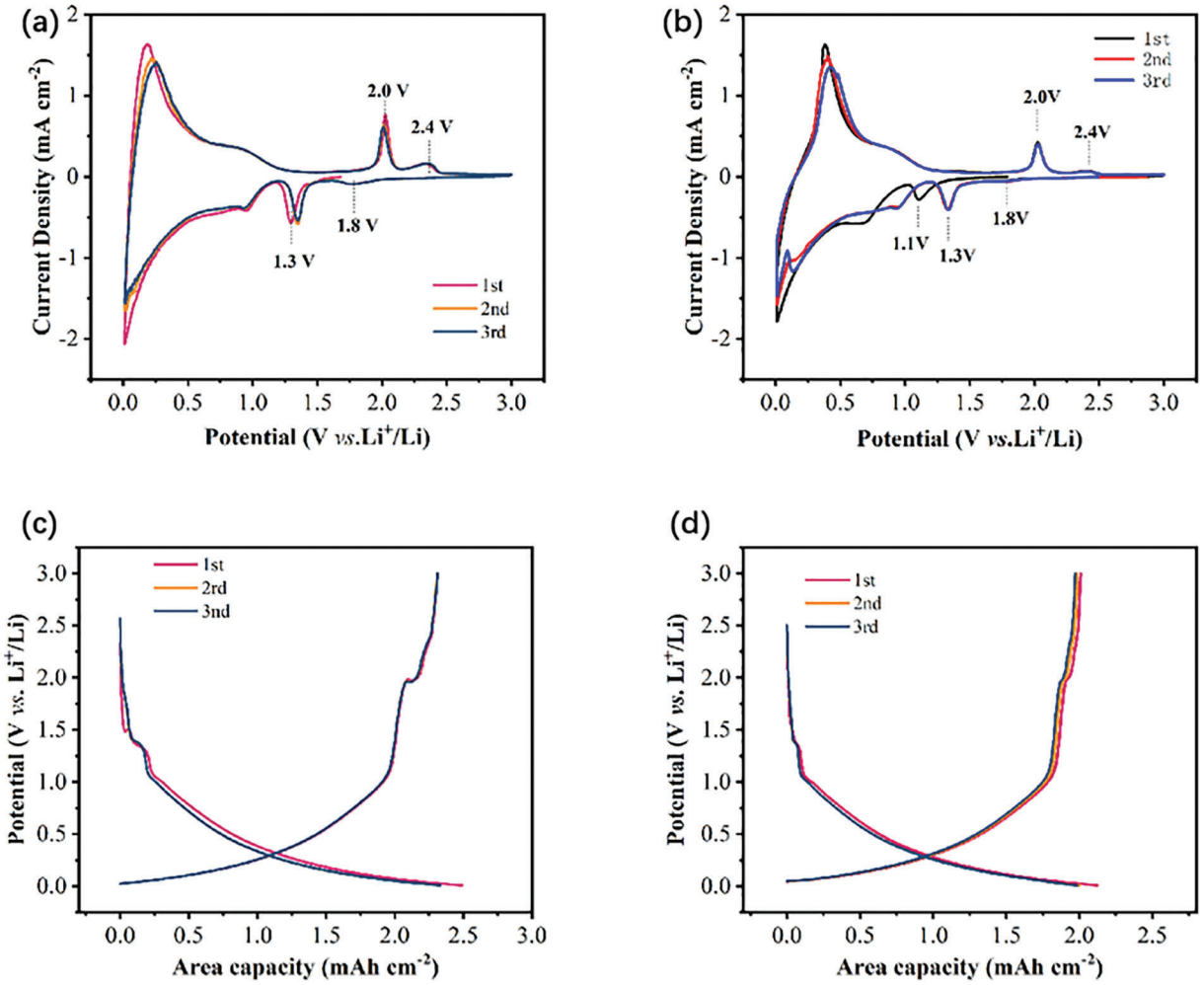

Figure 5: (a) The first three cycles CV curve of CoS NS@C/CFC and (b) CoS NS/CFC (scanning speed is 0.1 mV s^{-1}, voltage range is between 0.01 and 3 V); The first three charge-discharge curves of (c) CoS NS@C/CFC and (d) CoS NS/CFC (current density is 0.92 mA cm^{-2})

Electrochemical impedance spectroscopies (EIS) of CoS NS@C/CFC and CoS NS/CFC were measured to analyze their redox reaction kinetics. Both Nyquist curves comprise a semicircle from high to medium frequency originated from charge transfer resistance R_{ct}, and a near-linear region at low frequency area which is attributed to Warburg impedance (Fig. 7c) [8,43]. The charge transfer resistance of CoS NS/CC anode is about 127 Ω. After coating with the C-PDA film, the R_{ct} value of CoS NS@C/CFC reduces to about 89 Ω. And moreover, CoS NS@C/CFC also exhibits a smaller Warburg impedance than CoS NS/CFC, implying that Li^+ can solid diffuse faster within the former electrode. The D_{Li^+} can be calculated according to the following equations:

$$Z' = R_C + R_{ct} + \sigma\omega^{-1/2} \tag{3}$$

$$D_{Li^+} = \frac{R^2T^2}{2A^2n^4F^4C^2\sigma^2} \tag{4}$$

where R, T, A, F and C represent Gas Constant, temperature, area of the electrode, Faraday Constant and Li^+ concentration, respectively [44]. As shown in Fig. 7d, the σ value of CoS NS/CC and CoS NS@C/CFC are

400.1 and 100.5, while the calculated D_{Li}^{+} are 8.2 * 10^{-15} and 1.3 * 10^{-13} cm^2/s, respectively. The CoS NS@C/CFC anode exhibits lower σ value but higher Lithium diffusion coefficient than CoS NS/CC anode, suggesting the C-PDA film coating has a significant improvement in the Li^+ diffusion. Meanwhile, the layered nanosheet structure not only increases the interface area between active particles and electrolyte to greatly increase the transmission paths of lithium ions, but also shortens the transmission distance of lithium ions, both facilitating the ionic conduction and solid state diffusion [45–47].

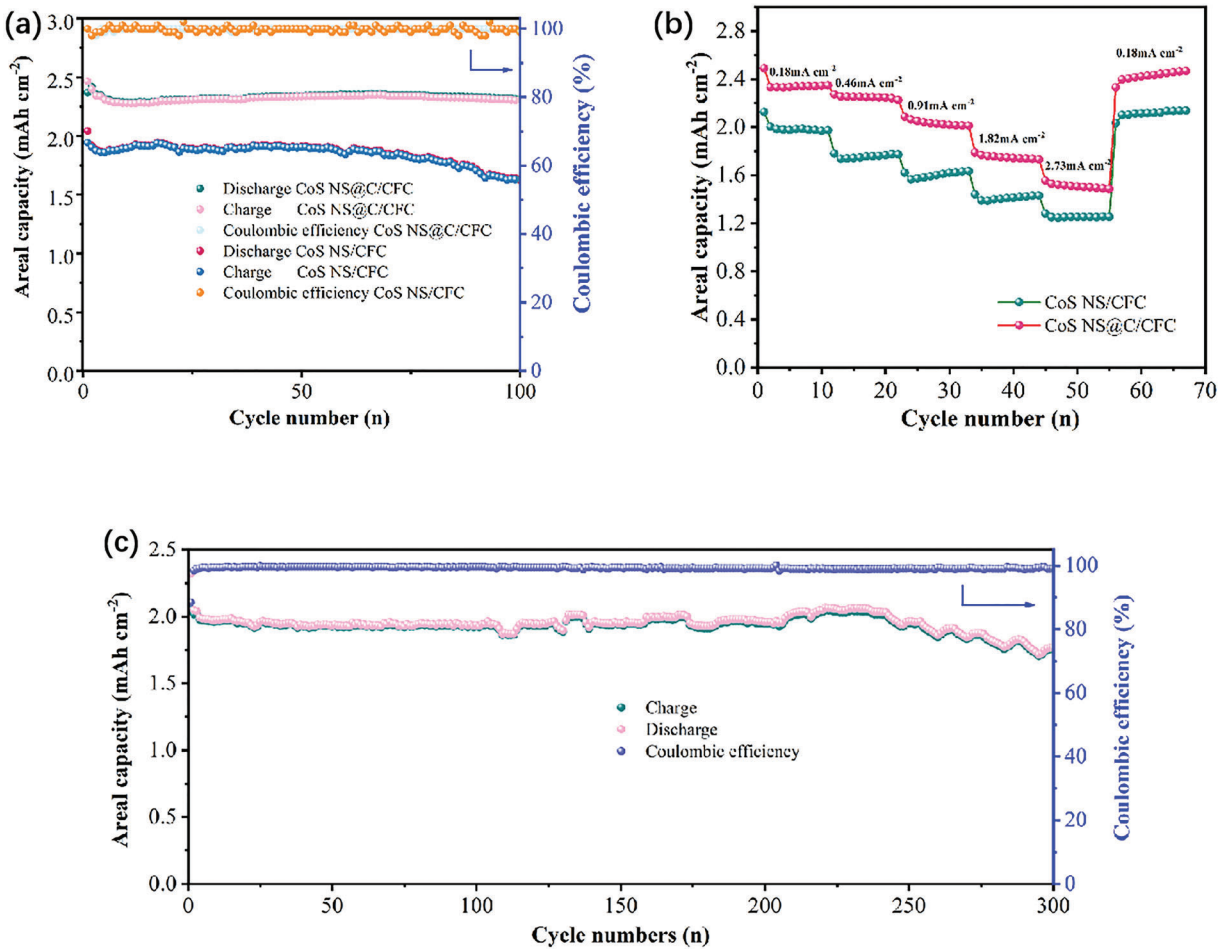

Figure 6: (a) Cycling stability at 0.91 mA cm^{-2} of CoS NS@C/CFC and CoS NS/CC anode and the corresponding Coulombic efficiency (b) Rate performance of CoS NS@C/CFC and CoS NS/CC anode at various current densities of 0.18, 0.46, 0.91, 1.82, and 2.73 mA cm^{-2} (c) Cycling stability at 1.82 mA cm^{-2} of CoS NS@C/CFC anode and the corresponding Coulombic efficiency

As mentioned above, the self-supporting CoS NS@C/CFC anode prepared by the hydrothermal reaction followed with carbon coating method exhibits large reversible areal capacity, high coulombic efficiency, superior rate performance and good cycle performance. The enhanced performance may be related to the synergistic effects of CoS NS, CFC substrate and the coated carbon film. Carbon Fiber Cloth not only improves the conductivity of this 3D structure and promotes the rapid electron transport during Li^+ insertion/extraction, but also contributes partial of the capacity. Effective carbon film coating can further improve the electron conduction and effectively relieve volume expansion. The CoS nanosheets expand

the interface area between active materials and electrolyte significantly, providing numerous sites for the charge-transfer reactions.

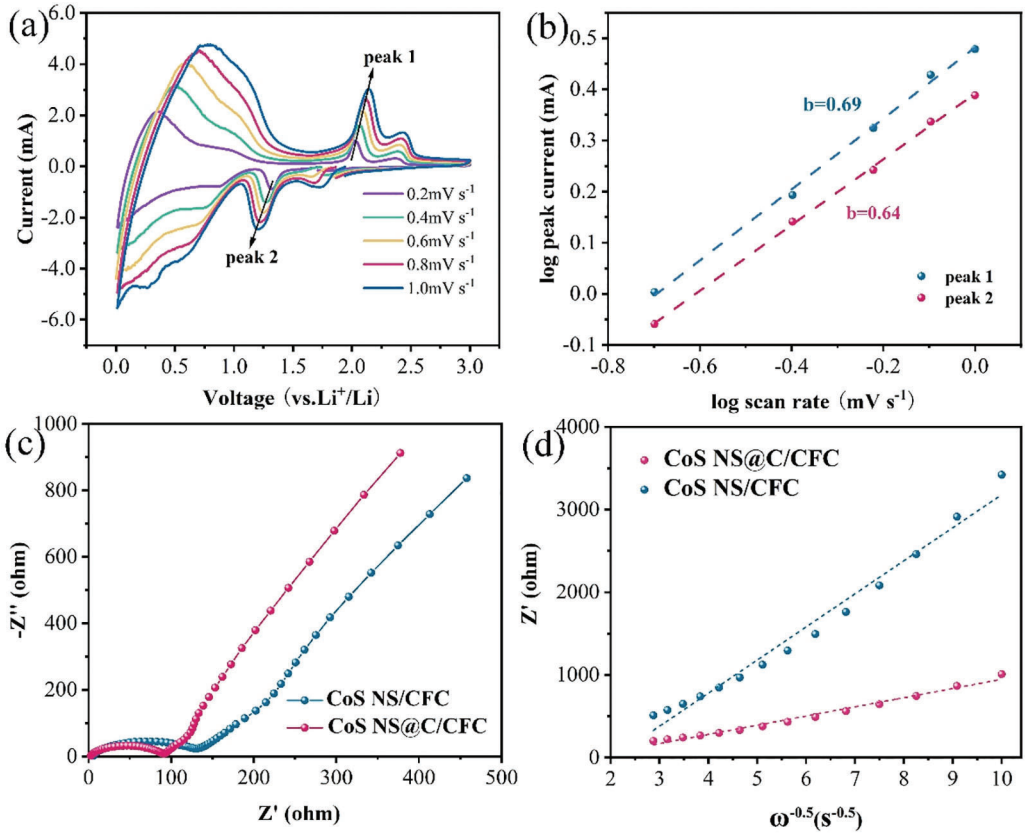

Figure 7: (a) CV curves of the CoS NS@C/CFC at various scan rates, (b) log i *vs*. log v plots (c) Nyquist plots of CoS NS@C/CFC and CoS NS/CFC anode. (d) Correlation between Z' and $\omega^{-1/2}$ in low frequencies derived from EIS results

4 Conclusion

In summary, a self-supporting CoS NS@C/CFC composite electrode is synthesized by the hydrothermal reaction followed by a carbon coating method, in which carbon-coated CoS nanosheets are firmly attached to the carbon fiber surface as an interconnected network with significantly expanded surface area. The large surface area ensures sufficient reaction sites for charge transfer reactions. Enough outer space of the CoS nanosheets can accommodate the volume variation. In addition, the coated carbon layer, combined with the CFC support, form a 3-D conductive network to enhance the electrons' conduction. Furthermore, CFC works as both support and active material, which further improves the available areal capacity. When being applied as the anode, the freestanding CoS NS@C/CFC electrode exhibits high areal capacity (2.5 at 0.15 mA cm^{-2}), excellent rate performance (1.6 at 2.73 mA cm^{-2}) and much improved cycle stability (87.5% capacity retention after 300 cycles). This greatly enhanced electrochemical performance can be attributed to the synergy effects provided by the CoS NS, coated carbon film and the CFC support.

Acknowledgement: None.

Funding Statement: This work was supported by the National Natural Science Foundation of China (Grant Nos. 21573109, 21206069), and the Priority Academic Program Development of Jiangsu Higher Education Institutions (PAPD).

Author Contributions: The authors confirm contribution to the paper as follows: study conception and design: Lianyuan Ji, Mingchen Shi; data collection: Lianyuan Ji, Mingchen Shi; analysis and interpretation of results: Lianyuan Ji, Mingchen Shi; draft manuscript preparation: Zengkai Feng and Hui Yang. All authors reviewed the results and approved the final version of the manuscript.

Availability of Data and Materials: Data is openly available in a public repository.

Conflicts of Interest: The authors declare that they have no conflicts of interest to report regarding the present study.

References

1. Bruce, P. G., Scrosati, B., Tarascon, J. M. (2008). Nanomaterials for rechargeable lithium batteries. *Angewandte Chemie International Edition, 47(16),* 2930–2946.
2. Wu, G., Liu, F., Li, S., Luo, N., Liu, Z. et al. (2023). Research on performance optimization of liquid cooling and composite phase change material coupling cooling thermal management system for vehicle power battery. *Journal of Renewable Materials, 11(2),* 707–730. https://doi.org/10.32604/jrm.2022.022276
3. Larcher, D., Tarascon, J. M. (2015). Towards greener and more sustainable batteries for electrical energy storage. *Nature Chemistry, 7,* 19–29.
4. Deng, D. (2015). Li-ion batteries: Basics, progress, and challenges. *Energy Science & Engineering, 3(5),* 385–418.
5. Chen, M., Liang, X., Wang, F., Xie, D., Pan, G. (2019). Self-supported VO_2 arrays decorated with N-doped carbon as an advanced cathode for lithium-ion storage. *Journal of Materials Chemistry A, 7(12),* 6644–6650.
6. Hao, J., Xu, X., You, H., Min, H., Yang, H. (2021). The free-standing cathode fabricated with nano-$CoSe_2$ embedded in mesoporous carbon nanosheets towards high performance Li/SeS_2 batteries. *Chemical Engineering Journal, 418(15),* 129475.
7. You, H., Zhang, W., Hao, J., Min, H., Yang, H. (2021). Freestanding $Fe_{0.4}CO_{8.6}S_8$ nanotube/nanosheet arrays on carbon cloth as a host for high-performance Li/SeS_2 batteries. *ACS Applied Energy Materials, 4(3),* 2496–2505.
8. Wang, Q., Zou, R., Xia, W., Ma, J., Qiu, B. A. et al. (2015). Facile synthesis of ultrasmall CoS_2 nanoparticles within thin N-Doped porous carbon shell for high performance lithium-ion batteries. *Small, 11(21),* 2511–2517.
9. Yang, Y., Xu, K., Zhao, B., Liu, N., Zhou, J. (2015). The bacteria absorption-based yolk-shell Ni3P-carbon @ reduced graphene oxides for lithium-ion batteries. *Journal of Renewable Materials, 9(5),* 855–865. https://doi.org/10.32604/jrm.2021.014525
10. Zou, R., Zhang, Z., Yuen, M. F., Sun, M., Hu, J. et al. (2015). Three-dimensional-networked $NiCo_2S_4$ nanosheet array/carbon cloth anodes for high-performance lithium-ion batteries. *NPG Asia Materials, 7,* e195.
11. Wang, R., Xu, C., Sun, J., Liu, Y., Gao, L. et al. (2014). Heat-induced formation of porous and free-standing MoS_2/GS hybrid electrodes for binder-free and ultralong-life lithium ion batteries. *Nano Energy, 8,* 8183–8195.
12. Chen, J., Cong, J., Chen, Y., Wang, Q., Yang, H. et al. (2019). MnS nanoparticles embedded in N,S co-doped carbon nanosheets for superior lithium ion storage. *Applied Surface Science, 508(1),* 145239.
13. Hua, G., Kong, S., Yong, W. (2014). NiS nanorods-assembled nanoflower grown on graphene: Morphology evolution and Li-ion storage application. *Journal of Materials Chemistry A, 2(36),* 15152–15158.
14. Wang, S., Ning, P., Huang, S., Wang, W., Fei, S. et al. (2019). Multi-functional NiS_2/FeS_2/N-doped carbon nanorods derived from metal-organic frameworks with fast reaction kinetics for high performance overall water splitting and lithium-ion batteries. *Journal of Power Sources, 436(1),* 226857.

15. Jiao, Z., Zhao, P., He, Y., Ling, L., Sun, W. (2019). Mesoporous yolk-shell CoS_2/nitrogen-doped carbon dodecahedron nanocomposites as efficient anode materials for lithium-ion batteries. *Journal of Alloys and Compounds, 809(15),* 151854.
16. Gu, Y., Xu, Y., Wang, Y. (2013). Graphene-wrapped CoS nanoparticles for high-capacity lithium-ion storage. *ACS Applied Materials & Interfaces, 5(3),* 801–806.
17. He, X., Bi, L., Li, Y., Xu, C., Lin, D. (2020). CoS_2 embedded graphitic structured N-doped carbon spheres interlinked by rGO as anode materials for high-performance sodium-ion batteries. *Electrochimica Acta, 332(1),* 135453.
18. Liao, S. Y., Cui, T. T., Zhang, S. Y., Cai, J. J., Zheng, F. Y. et al. (2019). Cross-nanoflower CoS_2 *in-situ* self-assembled on rGO sheet as advanced anode for lithium/sodium ion battery. *Electrochimica Acta, 326(5),* 134992.
19. Ma, X., Fang, K., Yang, X., Jiang, J., Meng, L. et al. (2020). Engineering of Co_9S_8–CoS nanoparticles encapsulated into N-doped graphitic carbon tubes for high-performance lithium storage. *Journal of Alloys and Compounds, 818(25),* 152859.
20. Lin, W., Huang, Y., He, G. (2018). Unique CoS hierarchitectures for high-performance lithium ion batteries. *Crystengcomm, 20(42),* 6727–6732.
21. Xiao, Y., Hwang, J. Y., Belharouak, I., Sun, Y. K. (2017). Superior Li/Na-storage capability of a carbon-free hierarchical CoS x hollow nanostructure. *Nano Energy, 32,* 320–328.
22. Du, Y., Zhu, X., Zhou, X., Hu, L., Dai, Z. et al. (2015). Co_3S_4 porous nanosheets embedded in graphene sheets as high-performance anode materials for lithium and sodium storage. *Journal of Materials Chemistry A, 3(13),* 6787–6791.
23. Yu, L., Yang, J. F., Lou, X. W. (2016). Formation of CoS_2 nanobubble hollow prisms for highly reversible lithium storage. *Angewandte Chemie, 55(43),* 13422–13426.
24. Xia, H., Li, K., Guo, Y., Guo, J., Xu, Q. et al. (2018). CoS_2 nanodots trapped within graphitic structured N-doped carbon spheres with efficient performances for lithium storage. *Journal of Materials Chemistry A, 6(16),* 7148–7154.
25. Wang, M., Wang, X., Yao, Z., Tang, W., Xia, X. et al. (2019). SnO_2 nanoflake arrays coated with polypyrrole on a carbon cloth as flexible anodes for sodium-ion batteries. *ACS Applied Materials & Interfaces, 11(27),* 24198–24204.
26. Zhang, C., Li, H., Zeng, X., Xi, S., Wang, R. et al. (2022). Accelerated diffusion kinetics in ZnTe/$CoTe_2$ heterojunctions for high rate potassium storage. *Advanced Energy Materials, 12(41),* 2202577.
27. Yan, Y., Wang, B., Yan, C., Kang, D. J. (2019). Decorating ZnO nanoflakes on carbon cloth: Free-standing, highly stable lithium-ion battery anodes. *Ceramics International, 45(13),* 15906–15912.
28. Peng, S., Han, X., Li, L., Zhu, Z., Cheng, F. et al. (2016). Unique cobalt sulfide/reduced graphene oxide composite as an anode for sodium-ion batteries with superior rate capability and long cycling stability. *Small, 12(10),* 1359–1368.
29. Gao, H., Zhou, T., Zheng, Y., Zhang, Q., Liu, Y. et al. (2017). CoS quantum dot nanoclusters for high-energy potassium-ion batteries. *Advanced Functional Materials, 27(43),* 1702634.
30. Zheng, F. C., Zhu, D. Q., Shi, X. H., Chen, Q. W. (2015). Metal-organic framework-derived porous $Mn_{1.8}Fe_{1.2}O_4$ nanocubes with an interconnected channel structure as high-performance anodes for lithium ion batteries. *Journal of Materials Chemistry A, 3(6),* 2815–2824.
31. Lian, Y., Xin, W., Zhang, M., Li, Y., Yang, L. et al. (2019). Low-content Ni-doped CoS_2 embedded within N, P-codoped biomass-derived carbon spheres for enhanced lithium/sodium storage. *Journal of Materials Science, 54,* 8504–8514.
32. Guo, Y., Gan, L., Shang, C., Wang, E., Wang, J. (2017). A cake-style CoS_2@MoS_2/RGO hybrid catalyst for efficient hydrogen evolution. *Advanced Functional Materials, 27(5),* 1602699.
33. Jin, R., Yang, L., Li, G., Chen, G. (2015). Hierarchical worm-like CoS_2 composed of ultrathin nanosheets as an anode material for lithium-ion batteries. *Journal of Materials Chemistry A, 3(20),* 10677–10680.
34. Pan, Y., Cheng, X., Huang, Y., Gong, L., Zhang, H. (2017). CoS_2 nanoparticles wrapping on flexible freestanding multichannel carbon nanofibers with high performance for Na-ion batteries. *ACS Applied Materials & Interfaces, 9(41),* 35820–35828.

35. Pan, Y., Cheng, X., Gong, L., Shi, L., Zhang, H. (2018). Nanoflower-like N-doped C/CoS_2 as high-performance anode materials for Na-ion batteries. *Nanoscale, 10(44),* 20813–20820.
36. Mao, Y. J., Chen, Y. T., Qin, J., Shi, C. S., Liu, E. Z. et al. (2019). Capacitance controlled, hierarchical porous 3D ultra-thin carbon networks reinforced prussian blue for high performance Na-ion battery cathode. *Nano Energy, 58,* 192–201.
37. Bruce, P. G., Freunberger, S. A., Hardwick, L. J., Tarascon, J. (2012). Li-O_2 and Li-S batteries with high energy storage. *Nature Materials, 11,* 19–29.
38. Shi, W., Zhu, J., Rui, X., Cao, X., Chen, C. H. et al. (2012). Controlled synthesis of carbon-coated cobalt sulfide nanostructures in oil phase with enhanced li storage performances. *ACS Applied Materials & Interfaces, 4(6),* 2999–3006.
39. Yang, Z., Wang, J., Wu, H. T., Kong, F. J., Yin, W. Y. et al. (2019). MOFs derived Co_1−S nanoparticles embedded in N-doped carbon nanosheets with improved electrochemical performance for lithium ion batteries. *Applied Surface Science, 479(15),* 693–699.
40. Luo, F., Ma, D., Li, Y., Mi, H., Zhang, P. et al. (2019). Hollow Co_3S_4/C anchored on nitrogen-doped carbon nanofibers as a free-standing anode for high-performance Li-ion batteries. *Electrochimica Acta, 299(10),* 173–181.
41. Augustyn, V., Simon, P., Dunn, B. (2014). Pseudocapacitive oxide materials for high-rate electrochemical energy storage. *Energy & Environmental Science, 7(5),* 1597–1614.
42. Zhang, S., Qiu, L., Zheng, Y., Shi, Q., Zhou, T. et al. (2021). Rational design of core-shell ZnTe@N-doped carbon nanowires for high gravimetric and volumetric alkali metal ion storage. *Advanced Functional Materials, 31(3),* 2006425.
43. Song, J., Zhang, C., Zhang, J., Zhou, H., Chen, L. et al. (2019). Construction of CoS_2-N-C sheets anchored on 3D graphene network for lithium storage performances. *Journal of Nanoparticle Research, 21,* 90.
44. You, H., Shi, M., Hao, J., Min, H., Yang, H. et al. (2020). A spongy mesoporous titanium nitride material as sulfur host for high performance lithium-sulfur batteries. *Journal of Alloys and Compounds, 823(15),* 153879.
45. Lin, X., Xue, D., Zhao, L., Zong, F., Duan, X. et al. (2019). *In-situ* growth of 1T/2H-MoS_2 on carbon fiber cloth and the modification of SnS_2 nanoparticles: A three-dimensional heterostructure for high-performance flexible lithium-ion batteries. *Chemical Engineering Journal, 356(15),* 483–491.
46. Xie, Q., Zhang, Y., Zhu, Y., Fu, W., Zhang, X. et al. (2017). Graphene enhanced anchoring of nanosized Co_3O_4 particles on carbon fiber cloth as free-standing anode for lithium-ion batteries with superior cycling stability. *Electrochimica Acta, 247(1),* 125–131.
47. Huang, J., Hou, D., Zhou, Y., Zhou, W., Li, G. et al. (2015). MoS_2 nanosheet-coated CoS_2 nanowire arrays on carbon cloth as three-dimensional electrodes for efficient electrocatalytic hydrogen evolution. *Journal of Materials Chemistry A, 3(45),* 22886–22891.

Supplementary Materials

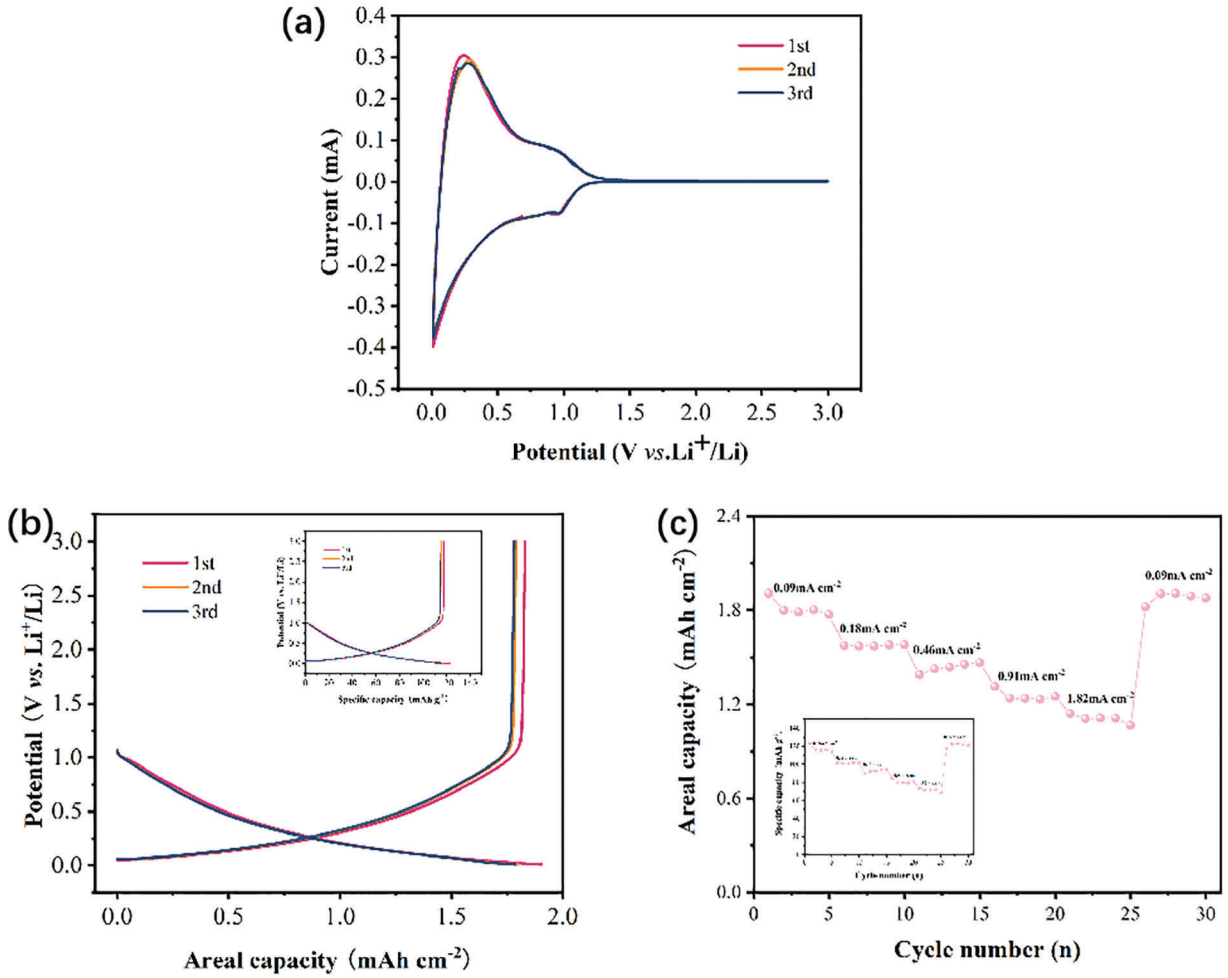

Figure S1: Electrochemical measurements of CC (a) CV curves of CC anode at a scan rate of 0.1 mV s^{-1} between 0.01 and 3.0 V (b) Discharge and charge voltage profiles of CC anode at a current density of 0.09 mA cm^{-2} for the first three cycles (c) The rate capability of CC anode

At the current density of 0.91 mA cm^{-2}, the average capacity of CFC, CoS NS/CFC and CoS NS@C/CFC are 1.254 mAh cm^{-2} (Fig. S1c), 1.604 mAh cm^{-2} (Fig. 6b) and 2.03 mAh cm^{-2} (Fig. 6b), respectively. The chosen CFC support presents the density of 15.5 mg/cm^2, while the loaded CoS NS and CoS NS@C are only around 1.3 ± 0.2 and 1.3 ± 0.2 mg/cm^2, respectively. Therefore, the specific capacity of CFC is calculated as around 80.9 mAh/g, while those of CoS NS and CoS NS@C are 292 and 597 mAh/g, respectively.

In this case, the lithium storage mechanism within CFC is the same as other carbonaceous materials as follows:

$xLi^+ + C + xe^- \rightleftharpoons Li_xC$ ($x \leq 0.0362$, calculated based on 80.9 mAh/g)

Even though the specific capacity of the CFC is not high, it contributes around 60% of the total capacity in the CoS NS@C/CFC composite electrode in this context since its mass occupies 92.3% of the total mass of the composite electrode. In this case, CFC works as both the active substance and the 3D skeleton in our current study.

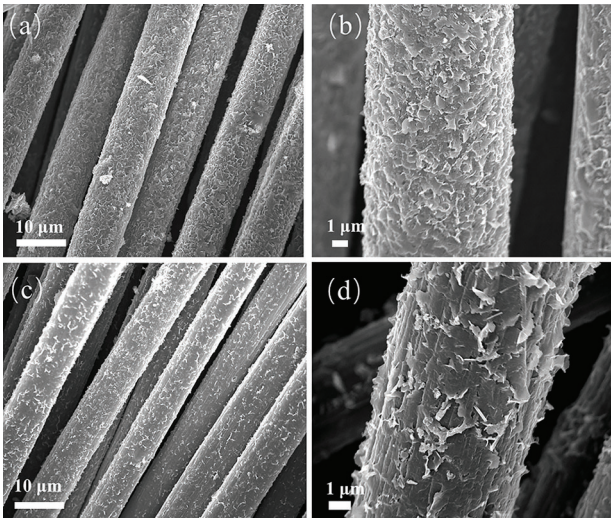

Figure S2: Images of (a–b) CoS NS@C/CFC and (c–d) CoS NS/CFC anode after 100 cycles

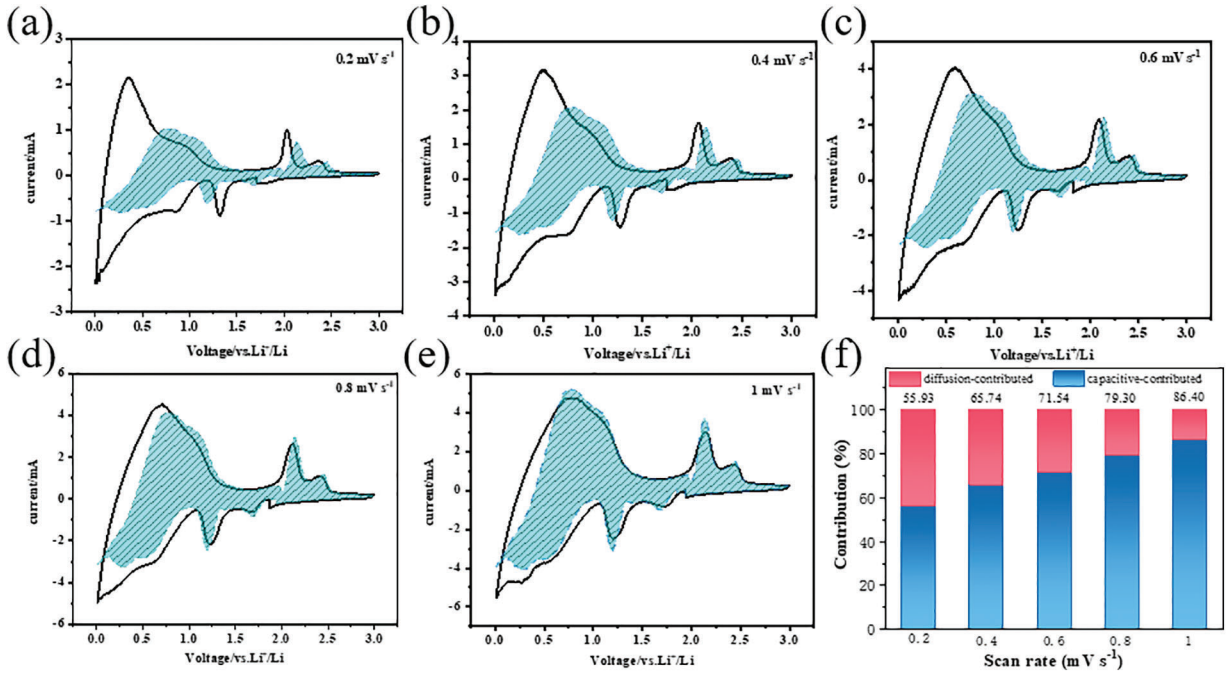

Figure S3: (a–e) Capacitive charge storage contribution (f) the percent of diffusion-contributed and capacitive-contributed capacities of CoS NS@C/CFC anode at different scan rates

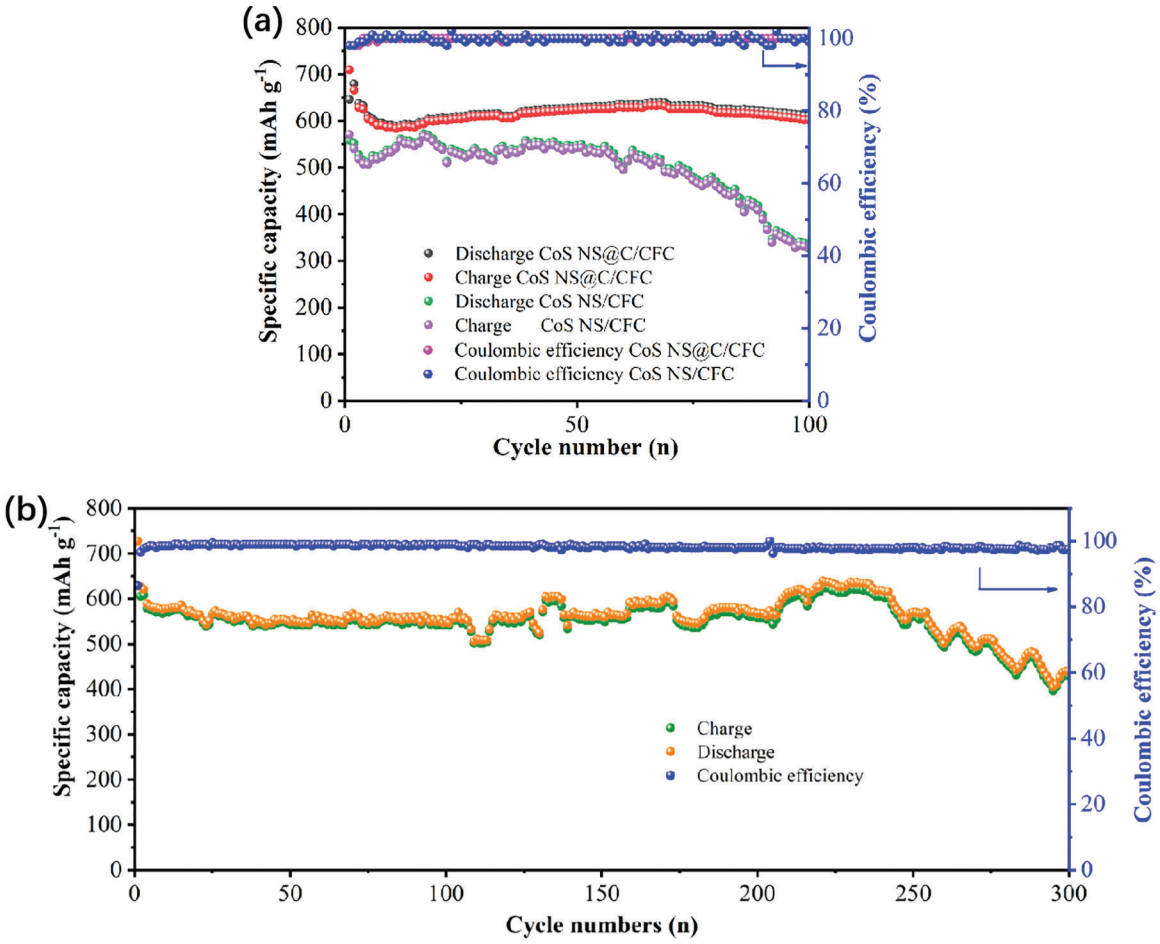

Figure S4: (a) Cycling stability at 0.91 mA cm^{-2} of CoS NS@C/CFC (Cobalt sulfide provides specific capacity with a load of 1.5 mg) and CoS NS/CC (Cobalt sulfide provides specific capacity with a load of 1.3 mg) anode and the corresponding Coulombic efficiency (b) Cycling stability at 1.82 mA cm^{-2} of CoS NS@C/CFC (Cobalt sulfide provides specific capacity with a load of 1.4 mg) anode and the corresponding Coulombic efficiency